



Contents lists available at ScienceDirect

# Computers and Electrical Engineering

journal homepage: [www.elsevier.com/locate/compeleceng](http://www.elsevier.com/locate/compeleceng)

## Enhancement of Low Illumination Images based on an Optimal Hyperbolic Tangent Profile<sup>☆</sup>

San Chi Liu<sup>a</sup>, Shilong Liu<sup>a</sup>, Hongkun Wu<sup>a</sup>, Md Arifur Rahman<sup>a</sup>, Stephen Ching-Feng Lin<sup>a</sup>, Chin Yeow Wong<sup>a</sup>, Ngaiming Kwok<sup>a,\*</sup>, Haiyan Shi<sup>b</sup>

<sup>a</sup> School of Mechanical and Manufacturing Engineering, The University of New South Wales, Sydney 2052, Australia<sup>b</sup> School of Mechanical and Electrical Engineering, Shaoxing University, Shaoxing, Zhejiang 312000, China

## ARTICLE INFO

## Article history:

Received 2 December 2016

Revised 16 August 2017

Available online xxx

## Keywords:

Contrast enhancement

Low illumination images

Optimum hyperbolic tangent mapping

Hybrid linear weighting

## ABSTRACT

Contrast enhancement is a critical pre-processing stage for many image based applications. It is frequently encountered that the illumination condition, while capturing the image, is imperfect. Specific algorithms have to be applied to restore these images from, for instance, the degradation due to low illumination. An adaptive enhancement method is developed here that tackles the image quality enhancement problem from an optimization perspective. In particular, the input image intensity is mapped to the output based on a weighted hybrid of a hyperbolic tangent and a linear profile. The mapping parameters are optimized, with regard to maximizing the image global entropy, by using the Golden Section Search algorithm for its implementation efficiency. Moreover, user interventions are not necessary. Better qualitative and comparable quantitative performances are obtained from experiments, with regard to the increase of brightness, information content and suppression of unwanted artifacts, as compared to recent profile mapping based methods.

© 2017 Elsevier Ltd. All rights reserved.

### 1. Introduction

The application of image processing technologies can be found in a large number of problem domains. In medical imaging, it is a requirement to enhance the captured endoscope images to facilitate illness diagnosis [1]. In remote sensing [2], image processing techniques are applied to restore degraded data. For surveillance systems, images with high resolution and contrast are required [3]. Furthermore, the wear states of machines can be investigated by using image based online ferrography [4]. In manufacturing automation, image processing is used to detect seams for guiding robot welding [5].

Due to increasing demands for high quality images, various image enhancement techniques were developed, each with its specific purpose. For instance, it may be required to boost the color saturation for a digital image to convey more truly information to the viewer [6]. Also, if it is needed to enhance the details of objects captured in an image, the unsharp masking filter can be applied [7]. The image contrast can be enhanced by using histogram based approaches [8,9]. Moreover, the amount of information carried in an image can be restored by making use of all the permitted intensity levels [10].

One of the challenging situations, where image processing techniques can be made use of, is the restoration of low illumination images. As illumination is an extrinsic factor to the camera and its effect cannot be precisely controlled when

<sup>☆</sup> Reviews processed and recommended for publication to the Editor-in-Chief by Area Editor Dr. E. Cabal-Yepez.

\* Corresponding author.

E-mail address: [nmkwok@unsw.edu.au](mailto:nmkwok@unsw.edu.au) (N. Kwok).

an image is captured, a class of techniques have been developed to address the difficulties in restoring the images. These include methods based on the reflectance model [11,12]. The use of intensity magnitude mappings, such as the gamma correction approach and its variants are frequently adopted [13–15]. There are also methods adopting nonlinear transfer of input to output intensities. For example, the mapping can be constructed based on local image characteristics [16,17]. The development of algorithms based on hybridization of the above-mentioned approaches have also been reported [18]. Moreover, adaptations of the original image features based on a trigonometric function to guide enhancements were proposed [19].

Although some satisfactory enhancement results can be obtained from the above-mentioned algorithms, they may not be applicable to a wide range of low illumination images. It is mainly due to the fact that these algorithms were designed with fixed parameters and adaptability and optimality were not addressed. In this paper, an adaptive and optimal low illumination image enhancement algorithm, Enhancement of Low Illumination Images based on an Optimal Hyperbolic Tangent Profile (ELIOHTP), is presented. The output image intensity is obtained from mapping its input through a nonlinear profile. A hyperbolic tangent function is adopted because of its well-known saturation characteristic where low intensities can be boosted. The mapping is also modified in a weighted sum with the original input to limit undesirable adjustments to high intensities. The proper function parameter is optimally obtained by using the Golden Section Search algorithm such that the global entropy contained in the output image is maximized. Test results have shown that the proposed algorithm outperforms qualitatively and is quantitatively comparable to other intensity mapping based algorithms.

The rest of this paper is organized as follows. In [Section 2](#), several classes of related work in profile based intensity mapping are reviewed. [Section 3](#) details the development of the proposed enhancement method for low illumination images. Experiments carried out are described, and results are discussed in [Section 4](#). A conclusion is drawn in [Section 5](#).

## 2. Related work

The enhancement of images captured in low illumination conditions is a challenging task because of the wide diversity of the environment conditions external to the camera. A possible strategy is to make use of the captured image intensity and map it to some desirable values to produce an output image of better quality. There are methods to tackle this problem including algorithms that make use of local statistics and nonlinear functions. Before presenting the proposed enhancement algorithm, a review of related work is given below. These include the multi-scale, statistics based, and hybrid approaches.

### 2.1. Multi-scale based approaches

One of the earlier researches in restoration of low illumination images adopts the multi-scale approach. Representative works include the Integrated Neighborhood Dependent Approach for Nonlinear Enhancement of Color Images (INDANE) [11], Adaptive and Integrated Neighborhood-Dependent Approach for Nonlinear Enhancement of Color Images (AINDANE) [12], and the Nonlinear Transfer Function-Based Local Approach for Color Image Enhancement (NTFLA) [16].

In the INDANE method [11], the input color image in red-green-blue (RGB) is first converted into the NTSC (YIQ) space and the Y-intensity image  $I \in [0, 1]$  is extracted. It is further processed to give an intermediate image

$$I_p = 0.5 \times (I^{0.24} + 0.5(1 - I) + I^2). \quad (1)$$

It is then convolved with a normalized Gaussian kernel with a standard deviation  $\sigma_c$ , that is

$$I_c(\mathbf{x}) = I(\mathbf{x}) \otimes G(\mathbf{g}, \sigma_c), \quad (2)$$

where

$$G(\mathbf{g}, \sigma_c) = \frac{1}{N} \exp\left(\frac{-(x - g_x)^2 + (y - g_y)^2}{2\sigma_c^2}\right), \quad (3)$$

and  $(g_x, g_y) \in \mathbf{g}$  is a local neighborhood centering at pixel coordinate  $\mathbf{x} = (x, y)$ , and  $x = 1, \dots, X$ ,  $y = 1, \dots, Y$  for an image of size  $X$ -by- $Y$ . The variable  $N$  is a normalization factor such that the elements in  $G(\mathbf{g}, \sigma_c)$  sum up to one, and  $\otimes$  is the convolution operator. The convolved image is divided by the intensity  $I(\mathbf{x})$  to generate a ratio  $r(\mathbf{x}) = I_c(\mathbf{x})/I(\mathbf{x})$ . The intermediate processed image is raised to the power of  $r(\mathbf{x})$ , giving

$$I_r(\mathbf{x}) = I_p(\mathbf{x})^{r(\mathbf{x})}. \quad (4)$$

The convolution, and power raising operations are repeated three times by using three different kernel scales determined by the standard deviation  $\sigma_c$  in  $G(\mathbf{g}, \sigma_c)$ . This repetitive process gives three power-raised images  $I_{r,i}(\mathbf{x})$  using  $\sigma_c, i$ ,  $i = 1, 2, 3$  and  $\sigma_c = [5, 20, 240]$ . Furthermore, the power-raised images are averaged, giving a guiding image as

$$I_g(\mathbf{x}) = \frac{1}{3} \sum_i I_{r,i}(\mathbf{x}), \quad i = 1, 2, 3. \quad (5)$$

Another scaling factor is formed, giving  $s(\mathbf{x}) = I_g(\mathbf{x})/I(\mathbf{x})$ . This factor is used to generate the enhanced image,  $I_{en}(\mathbf{x}) = \{R_{en}, G_{en}, B_{en}\}(\mathbf{x})$ , from adjusting the RGB components as

$$R_{en}(\mathbf{x}) = s \times R(\mathbf{x}), \quad G_{en}(\mathbf{x}) = s \times G(\mathbf{x}), \quad B_{en}(\mathbf{x}) = s \times B(\mathbf{x}). \quad (6)$$

A similar approach was adopted for the AINDANE algorithm [12]. It generates the intermediate image using a different formula

$$I_p(\mathbf{x}) = 0.5 \times (I(\mathbf{x})^{0.25+0.75z} + 0.4(1 - I(\mathbf{x}))(1 - z) + I^{2z}(\mathbf{x})). \quad (7)$$

This process depends on the coefficient  $z$ , which is determined from the probability distribution function (pdf) of the input image  $I(\mathbf{x})$ . An index  $L \in [1, 256]$  is defined such that the cumulative distribution function (cdf) of the intensity at this  $L$ th level is 0.1. The coefficient  $z$  is obtained from

$$z = \begin{cases} 0, & L \leq 50 \\ (L - 50)/100, & 50 < L \leq 150 \\ 1, & L > 150. \end{cases} \quad (8)$$

Another modification from INDANE is that the power to raise  $I_p(\mathbf{x})$  is derived from  $\epsilon = (I_c/I)^\gamma$ , where

$$\gamma = \begin{cases} 3, & \sigma \leq 3 \\ (27 - 2\sigma)/7, & 3 < \sigma \leq 10 \\ 1, & \sigma > 10, \end{cases} \quad (9)$$

and  $\sigma$  is the standard deviation of the intensity image  $I(\mathbf{x}) \in [0, 255]$ . The image resulting from rising to power  $\epsilon$  is then  $I_r(\mathbf{x}) = I_p^\epsilon(\mathbf{x})$ . The rest of the algorithm is the same as the procedure given in INDANE except that the Gaussian kernel parameters are chosen as  $c = [5, 20, 120]$ .

A later work was developed on the basis of the above two algorithms. In NTFLA [16], the formulation for the initial intensity processing is changed to

$$I_p(\mathbf{x}) = 0.5 \times (I(\mathbf{x})^{0.25+0.75z} + 0.4(1 - z)(1 - I(\mathbf{x})) + I(\mathbf{x})(1 - z)). \quad (10)$$

An alternative scheme in obtaining the  $z$  coefficient was adopted. A sliding window of size  $N \times N$ , stepping through  $n \times n$  pixels, is used to collect image statistics for calculating the cdf. The collection of  $z$  coefficient from each sliding window is up-sampled to the size of the image given a pixel-to-pixel correspondence. The rest of the enhancement processes are the same as INDANE and AINDANE. It should be noted that NTFLA derives the intensity by converting the RGB space to the hue-saturation-value (HSV) space. Hence, no color adjustment is implemented in NTFLA, where the processed intensity image replaces the V-component in HSV and is then converted back to the RGB space as the final output.

## 2.2. Statistics based approaches

It can be observed that in a low illumination image, a major portion of pixels would have low intensities. This situation can be well represented in the image statistics. Methods making use of intensity probability distributions include the Efficient Contrast Enhancement using Adaptive Gamma Correction and Cumulative Intensity Distribution (AGCCID) [13], and the Minimum Mean Brightness Error Contrast Enhancement of Color Images using Adaptive Gamma Correction with Color Preserving Framework (AGCCPF) [15].

In the AGCCID method [13], the input color image is converted to a normalized gray-level image  $I(\mathbf{x}) \in [0, 1]$ . The pdf is constructed and its minimum  $\text{pdf}_{\min}$  and maximum  $\text{pdf}_{\max}$  values are determined. The pdf is further modified according to

$$\widehat{\text{pdf}}(L) = \text{pdf}_{\max} \left( \frac{\text{pdf}(L) - \text{pdf}_{\min}}{\text{pdf}_{\max} - \text{pdf}_{\min}} \right)^\alpha, \quad (11)$$

where  $\alpha$  is the power factor. Then the cdf is calculated from

$$\text{cdf}(L) = \sum_{l=1}^L \widehat{\text{pdf}}(l), \quad L = 1, \dots, 256. \quad (12)$$

Finally, the input intensity is mapped to the output by

$$\mathbf{J}(L) = \mathbf{I}(L)^{1-\text{cdf}(L)}. \quad (13)$$

The above method was further extended in the AGCCPF algorithm [15]. A modification is made on the generation of the pdf. Let the pdf of the input intensity be  $\text{pdf}_i(L)$ , it is weighted, using the factor  $\theta$ , with a uniform  $\text{pdf}_u(L)$  to give

$$\widehat{\text{pdf}}(L) = \theta \text{pdf}_i(L) + (1 - \theta) \text{pdf}_u(L). \quad (14)$$

The weighted  $\widehat{\text{pdf}}(L)$  is then used to generate the associated cdf to map the input to the intermediate image  $\tilde{\mathbf{I}}$  as given by the AGCCID algorithm. A further step was proposed in AGCCPF to derive the final output from using an additional factor  $\delta$ , giving

$$\mathbf{J}(L) = \delta \tilde{\mathbf{I}}(L) + (1 - \delta) \mathbf{I}(L). \quad (15)$$

### 2.3. Hybrid approaches

In addition to the classes of methods discussed above, hybrid approaches have also been reported in the literature. These include the Space Variant Luminance Map-Based Color Image Enhancement (SVLM) [18], and Locally Tuned Inverse Sine Nonlinear Technique for Color Image Enhancement (LTISN) [19].

In SVLM [18], an alternative process was carried out to handle the multi-scale convolution operation. In order to reduce the computation time, the gray-level image is down sampled three times and the convolved images are averaged, that is,

$$\mathbf{S}_v = \frac{1}{4} \sum_{i=1}^4 \mathbf{I}_{c,i}, \quad (16)$$

where  $\mathbf{I}_{c,i} = \mathbf{I}_{d,i} \otimes G(\mathbf{g}, c_i)$  is the convolved and up-sampled image of original sizes. The variable  $\mathbf{I}_{d,i}$  is the down sampled image of half the size of a preceding image. Note that the original gray-level image is  $\mathbf{I}_{d,1}$  and there is no down- and up-sampling.

A factor is obtained from a power law as  $\mathbf{O} = \mathbf{I}^\lambda$ , where  $\lambda = \alpha^{1-2\mathbf{S}_v}$ . Another factor is further defined as  $\mathbf{S} = \mathbf{O}^\epsilon$ , where  $\epsilon = (\mathbf{S}_v/\mathbf{O})^\gamma$ . The coefficient  $\gamma$  is obtained from the procedure given in AINDANE.

The LTISN method [19] follows the main procedures given in INDANE and AINDANE with the exception of a procedure that generates an intermediate processed image, that is

$$\mathbf{I}_p = \frac{2}{\pi} \sin^{-1}(\mathbf{I}^q), \quad (17)$$

where  $q$  is a locally adaptive tunable parameter and defined using

$$\mathbf{q} = \tan\left(\frac{\bar{I}\pi}{2.25}\right) + \beta. \quad (18)$$

The factor  $\beta$  is determined when the mean intensity  $\bar{I}$  is at 0.2.

### 2.4. Discussion

There have been some satisfactory results obtained from applying the aforementioned algorithms. However, their general applicability is the major shortcomings. It is largely due to the fact that these algorithms were not designed for application generality and their procedures are unnecessarily complicated. In particular, the parameter settings were fixed irrespective of image contents.

For example, in the INDANE algorithm the intermediate processed image is obtained as in Eq. (1). It is unclear that how the convolution kernel is chosen with  $c = [5, 20, 240]$ . Similarly, in AINDANE, the determination of coefficients  $z$  and  $\gamma$  in Eqs. (8) and (9) is dependent on fixed thresholds. Furthermore, the use of power law modification in the intensity using coefficient  $\epsilon$  is ambiguous. In NTFLA, the choices of the window size  $N \times N$  and the shift interval  $n \times n$  are not optimized. These design philosophies, to a certain extent, cannot guarantee that the obtained results are solidly supported.

In the AGCCID and AGCCPF approaches, it is not known how the power factor  $\alpha$  can be optimally determined. Furthermore, it is an open question in AGCCPF to choose the weighting parameters  $\theta$  and  $\delta$ , see Eqs. (14) and (15). The performances of these approaches are thus not guaranteed.

The SVLM method addresses the multi-scale problem by carrying out down- and up-sampling to improve computation efficiency. However, there are several stages of power law adjustments on the intensity needed. Hence, implementation efficiency is not ensured. In LTISN, there was no description on the manner in which the power factor is determined from a tangent function and a fixed coefficient.

The review has thus revealed the need for an algorithm that can be operated with true adaptability and minimum parameter settings. Hence, an algorithm that can fulfill the above objectives is developed. The algorithm includes a search routine that determines the optimal parameters aiming at maximizing the information that can be extracted from low illumination images. The details are presented in the next section.

## 3. Enhancement of Low Illumination Image

The proposed approach, Enhancement of Low Illumination Images based on an Optimal Hyperbolic Tangent Profile (ELIO-HTP), aims at restoring images captured under low illuminations. In particular, the algorithm is designed with simplicity and optimality. In [20], symmetrical hyperbolic tangent profiles were designed to help compress image intensity in the extreme light and dark regions to minimize artifact generation. Here, a different hyperbolic tangent function is instead chosen for primary intensity mapping across all three color channels. The mapping is further weighted linearly with the input intensity such that changes at high intensities are not encouraged. This weighting is based on the input intensity, thus removing the need for user specified fixed parameters. In addition, the scale of the hyperbolic tangent function is optimally determined from the Golden Section Search algorithm to ensure true adaptability to different image contents.

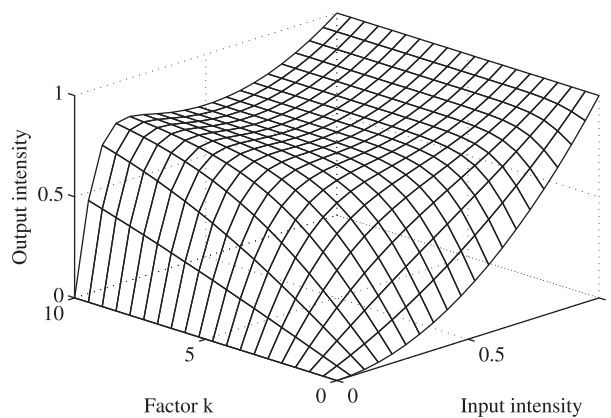


**Fig. 1.** Relationship between input/output intensity and gain factor  $k$ .

### 3.1. Input–output mapping function

Let the input color image be

$$\mathbf{I}(\mathbf{x}) = \mathbf{RGB}(\mathbf{x}) = \{R(\mathbf{x}), G(\mathbf{x}), B(\mathbf{x})\}, \quad (19)$$

where  $R(\mathbf{x}) \in [0, 1]$ ,  $G(\mathbf{x}) \in [0, 1]$ , and  $B(\mathbf{x}) \in [0, 1]$  are the RGB component intensities for a pixel located in the image coordinate  $(\mathbf{x})$ , and  $x = 1, \dots, X$ ,  $y = 1, \dots, Y$ .

The objective is to boost pixels of low intensity to a higher value for the Enhancement of Low Illumination Images. To achieve this, the hyperbolic tangent function is adopted as a nonlinear mapping [21], where

$$\tanh(\phi) = \frac{1 - \exp(-2\phi)}{1 + \exp(-2\phi)}. \quad (20)$$

If the variable  $\phi$  is set as a scaled version of the input intensity, that is,  $\phi = k \times \text{RGB}$ , the resultant mapped intensity is different for each level. From Eq. (20), it can be observed that if  $\phi \rightarrow 0$ , then  $\tanh(0) \rightarrow 0$ . If  $\phi \rightarrow 1$  and  $k = 3$ , then  $\tanh(3) \rightarrow 0.9951 \approx 1$ . Similarly, if  $\text{RGB} = 0.5$  and  $k = 3$ , then  $\tanh(1.5) \rightarrow 0.9051 > 0.5$ . Hence, there is an increase in the mapped output for low intensities while there is saturation for high intensities.

It can be observed that when the input intensity is zero, the mapped output is zero. On the other hand, if the input intensity is one, the output is limited to one. Hence, the permitted dynamic range is preserved while the magnitude of increase in intensity is dependent on the chosen scaling factor  $k$ .

A reduction on the boosting of high intensities is carried out using a weighted sum with the input intensity, giving the weighted output as

$$\mathbf{RGB}_w(\mathbf{x}) = \mathbf{w} \times \mathbf{RGB}(\mathbf{x}) + (1 - \mathbf{w}) \times \tanh(k \times \mathbf{RGB}(\mathbf{x})). \quad (21)$$

In order to impose equal adjustments to each color component in order to reduce any undesirable color distortions, the weighting coefficient  $w(\mathbf{x})$  is taken from the average of the color components,

$$\mathbf{w} = \{w(\mathbf{x})\} = \frac{1}{3} \sum_c \mathbf{RGB}_c(\mathbf{x}), \quad (22)$$

where  $c = \{R, G, B\}$  denotes the color component.

Furthermore, in order to ensure that the full intensity dynamic range is used, the weighted image is processed using a dynamic range stretching, that is

$$\widehat{\mathbf{RGB}}_s(\mathbf{x}) = \frac{\mathbf{RGB}_w(\mathbf{x}) - \mathbf{RGB}_{\min}}{\mathbf{RGB}_{\max} - \mathbf{RGB}_{\min}}, \quad (23)$$

where  $\mathbf{RGB}_{\min} = \min_{x,y}\{\mathbf{RGB}_w(\mathbf{x})\}$ ,  $\mathbf{RGB}_{\max} = \max_{x,y}\{\mathbf{RGB}_w(\mathbf{x})\}$ . Note that the minimum and maximum operators are taken for all pixel color components. The mapped output in accordance with the input intensity and the scaling factor  $k$  are shown in Fig. 1.

It can be seen from the figure that the mapping depends both on the input intensity and the scaling factor. When  $k = 0$ , the mapping attenuates the mid-level intensities. On the other hand, when  $k > 5$ , the mapped output at the low intensity range is larger than the mid-level; thus generating an intensity reversion and would create undesirable artifacts on the output image. Therefore, a proper choice of the factor  $k$  is needed for both providing enhancement and the reduction of artifacts.

### 3.2. Parameter optimization

The problem, deriving the proper scaling factor, is treated from the optimization perspective. Since there is only one variable, namely the gain factor  $k$ , to be optimized, the efficient Golden Section Search algorithm is adopted [7]. An iterative loop is invoked, maximizing the image information content measured in entropy, given as

$$\mathcal{J} = - \sum_{i=1}^{255} p(i) \log_2(p_i), \quad (24)$$

where  $p(i)$  is the probability that intensity level  $i$  appears in the processed image. Note that the entropy is calculated for all color components. This objective function is adopted because high entropy indicates that more permitted intensity levels are being made use of to carry the scene information captured in the image. The search terminates when the change of the desired scaling factor  $k$  in consequent iterations is within a small tolerance. This process is given in [Algorithm 1](#).

---

#### **Algorithm 1** Optimal processing of image enhancement.

---

```

Input: input image RGB
Output: optimally enhanced image RGBs*
Set iteration coefficient  $\rho = 0.5 \times (\sqrt{5} - 1) = 0.628$ , scaling factor tolerance  $\tau = 0.01$ 
Set initial scaling factor lower and upper limits  $k_L = 0.1$ ,  $k_H = 5$ , range  $\Delta k = k_H - k_L$ 
Set initial trial thresholds;  $k_1 = k_L + (1 - \rho)\Delta k$ ,  $k_2 = k_L + \rho\Delta k$ 
Evaluate initial objective functions;  $\mathcal{J}_1(k_1)$  of  $\mathcal{J}_2(k_2)$  using equations (21) to (24).
while  $\Delta k > \tau$  do
    if  $\mathcal{J}_1 > \mathcal{J}_2$  then
        Set  $k_H = k_2$ ,  $\Delta k = k_H - k_L$ ,  $k_1 = k_L + (1 - \rho)\Delta k$ ,  $k_2 = k_L + \rho\Delta k$ ,  $\mathcal{J}_2 = \mathcal{J}_1$ 
        Evaluate objective function  $\mathcal{J}_1(k_1)$  of enhancedimage RGBs,1( $k_1$ )
    else
        Set  $k_L = k_1$ ,  $\Delta k = k_H - k_L$ ,  $k_1 = k_L + (1 - \rho)\Delta k$ ,  $k_2 = k_L + \rho\Delta k$ ,  $\mathcal{J}_1 = \mathcal{J}_2$ 
        Evaluate objective function  $\mathcal{J}_2(k_2)$ , enhancedimage RGBs,2( $k_2$ )
    end if
end while
Return optimally enhanced image  $\text{RGB}_s^* = 0.5 \times (\text{RGB}_{s,1}(k_1) + \text{RGB}_{s,2}(k_1))$ 
```

---

Based on this search routine, the optimal setting of the scaling factor  $k$  is ensured. Consequently, the processed image is also optimum in the sense that the maximum information content is carried in the output image. This also means that the degradation due to low illumination is reduced.

### 3.3. Complexity analysis

Parameter settings in ELIOHTP is an optimization process. As indicated in [Algorithm 1](#), the optimal parameter is determined through iterations. In particular, the search domain reduces by the ratio  $\rho = 0.628 < 1$  with respect to its initial range  $\Delta k^0 = k_H^0 - k_L^0$ . After  $n$  iterations, the search range reduces to  $\Delta k^0 \rho^n$ . If we terminate the search at iteration  $N$  when the reducing range is less than threshold  $\tau$ , then the number of iterations can be obtained from

$$N = \left\lceil \frac{\log(\tau/\Delta k^0)}{\log \rho} \right\rceil = \left\lceil \frac{\log(0.01/(5 - 0.1))}{\log 0.628} \right\rceil = \lceil 13.3151 \rceil = 14, \quad (25)$$

where  $\lceil \cdot \rceil$  is the integer-round-up operator. It can be seen that using the Golden Section Search algorithm in ELIOHTP, only a small number of objective function evaluations are needed.

On the other hand, there are iterative optimization algorithms that can be used to obtain the optimal setting such as the harmony search (HS) [22]. Furthermore, nature-inspired algorithms including the metaheuristic bat-inspired algorithm (BAT) [23] and the artificial bee colony (ABC) algorithm [24] can be employed. Unlike the golden section search, they are multi-agent based iteration algorithms. For the same termination threshold to give the required parameter precision, i.e. the same specified  $\tau$ , it is not known how many iterations would be needed. In addition, there are multiple objective function evaluations because of the multi-agent nature of these algorithms. Hence, their computational complexities are much higher than the golden section search algorithm. It should also be noted that all these algorithms are able to obtain the optimal parameter and the results from ELIOHTP are the same. However, an efficient algorithm such as golden search is more desirable.

## 4. Experiment

The proposed Enhancement of Low Illumination Images based on an Optimal Hyperbolic Tangent Profile (ELIOHTP) algorithm is tested in experiments using a collection of 100 color images. These images are captured under a variety of

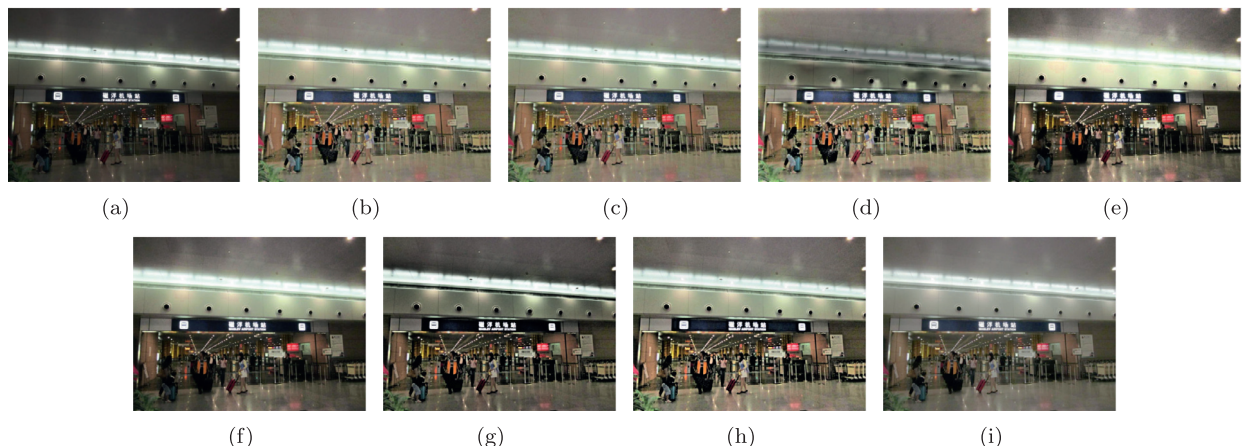


**Fig. 2.** Test image 1. (a) Input, (b) INDANE, (c) AINDANE, (d) NTFLA, (e) AGCCID, (f) AGCCPF, (g) SVLM, (h) LTISN, (i) ELIOOHTP.

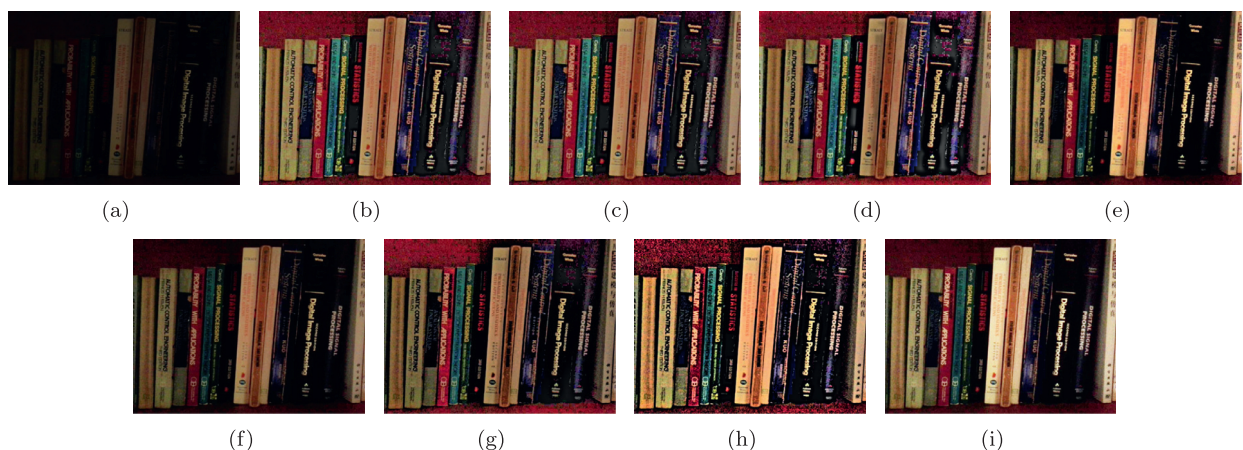


**Fig. 3.** Test image 2. (a) Input, (b) INDANE, (c) AINDANE, (d) NTFLA, (e) AGCCID, (f) AGCCPF, (g) SVLM, (h) LTISN, (i) ELIOOHTP.

illumination conditions as well as indoor and outdoor environments. These images are stored in the 8-bit JPEG format, and sized in  $360 \times 480$  pixels for landscape orientations,  $480 \times 360$  for portrait orientations.

The ELIOOHTP is compared with the methods reviewed. These include the INDANE, AINDANE, NTFLA, AGCCID, AGCCPF, SVLM, and the LTISN. The results are evaluated both qualitatively and quantitatively using common evaluation criteria. These include the entropy, mean brightness, global contrast, and local gradient measures.

#### 4.1. Qualitative analysis

Fig. 2 shows the various enhanced images obtained from the different algorithms. The input image is a typical indoor public area where the illumination strength is not specially designed for image capturing. Results from INDANE (Fig. 2(b)), AINDANE (Fig. 2(c)), and NTFLA (Fig. 2(d)) contains over-enhancements where the images appear too bright. On the other hand, results from AGCCID (Fig. 2(e)), AGCCPF (Fig. 2(f)), and SVLM (Fig. 2(g)) are under-enhanced where there are regions too dark. The result from LTISN (Fig. 2(h)), has both low and high intensity regions exaggerated and object details are lost. The result from ELIOOHTP (Fig. 2(i)), is able to provide the boost in low illumination regions while maintain object details.

The input image shown in Fig. 3 is an extreme low illumination image. An inspection on the results from INDANE (Fig. 3(b)), AINDANE (Fig. 3(c)), NTFLA (Fig. 3(d)), SVLM (Fig. 3(g)), and LTISN (Fig. 3(h)), all indicate the undesirable amplification of noisy backgrounds. In the contrary, results from AGCCID (Fig. 3(e)) and AGCCPF (Fig. 3(f)) are too dark. The best qualitative result is obtained from the ELIOOHTP method shown in Fig. 3(i).

An image of normal illumination and its enhancement results are show in Fig. 4. In this case, results from AGCCID (Fig. 4(e)), SVLM (Fig. 4(g)), and LTISN (Fig. 4(h)) are too bright. On the other hand, results from NTFLA (Fig. 4(d)), and AGCCPF (Fig. 4(f)) contain noticeable artifacts. The performance of the ELIOOHTP method (Fig. 4(i)) is not affected by different image contents such as those in normal illumination conditions.

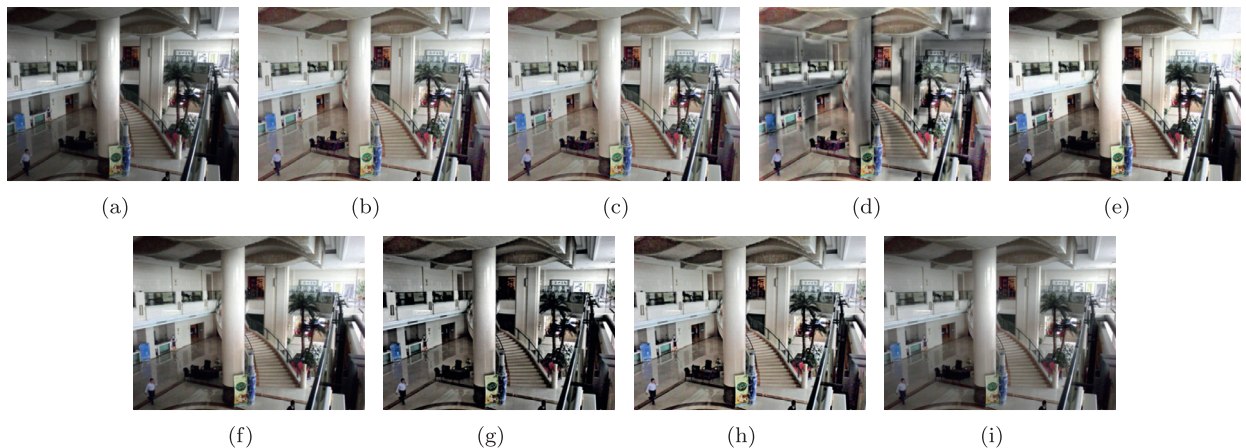


**Fig. 4.** Test image 3. (a) Input, (b) INDANE, (c) AINDANE, (d) NTFLA, (e) AGCCID, (f) AGCCPF, (g) SVLM, (h) LTISN, (i) ELIOOHTP.

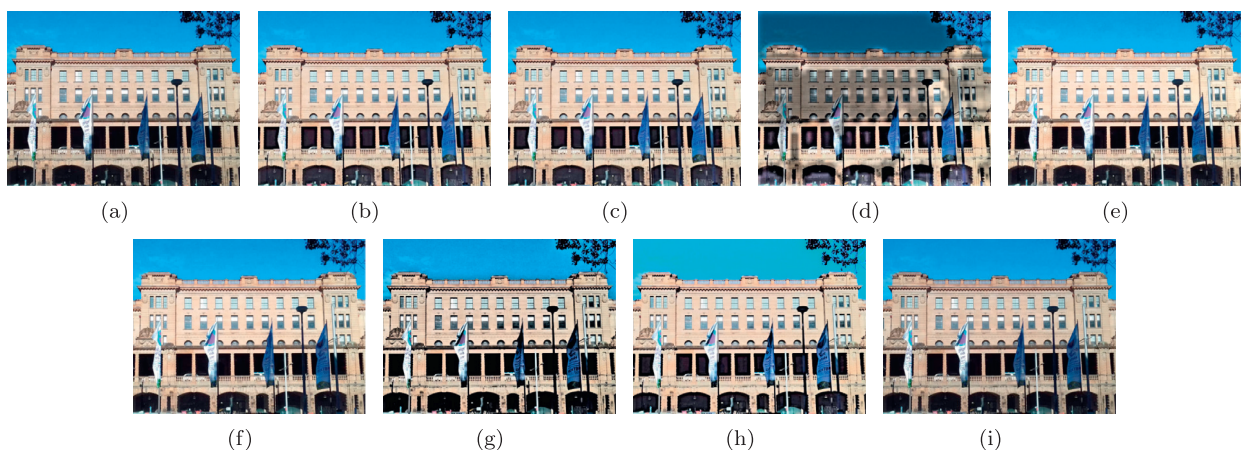


**Fig. 5.** Test image 4. (a) Input, (b) INDANE, (c) AINDANE, (d) NTFLA, (e) AGCCID, (f) AGCCPF, (g) SVLM, (h) LTISN, (i) ELIOOHTP.

The test image shown in Fig. 5 is a high illumination image. Results from NTFLA contains artifacts as found in other test cases. Images obtained from AGCCPF and LTISN are over-enhanced where the resultant images are too bright. All other tested methods, including ELIOOHTP produce satisfactory results qualitatively.

Test cases for medical images and their results are shown in Figs. 6 and 7. These images are obtained from Open Access Biomedical Image Search Engine, [https://openi.nlm.nih.gov/detailedresult.php?img=MPX1057\\_sympic58271&req=4](https://openi.nlm.nih.gov/detailedresult.php?img=MPX1057_sympic58271&req=4). The CT-scan image in Fig. 6 has a dark background and objects of interests appear in different gray scale magnitudes. All methods, except ELIOOHTP, produce unwanted viewing artifacts (upper left of the image) and cause interferences to the diagnostic process. The X-ray images having higher brightness are depicted in Fig. 7. Artifacts are observed from the NTFLA and SVLM results. There is over-enhanced brightness from other methods that lead to losses of details especially in the mid-bottom part of the images. The result from ELIOOHTP does not contain this drawback.

The qualitative analysis indicates that, algorithms designed with fixed parameters are not performing well for images of varied illumination conditions. Because of their designs, under- and over-enhancement occurs as well as unwanted artifacts are generated.

#### 4.2. Quantitative analysis

The performance of the proposed ELIOOHTP method is further evaluated quantitatively using four popular image quality criteria [7] and two recent image sharpness metrics [25,26]. These measures are focused on the information content carried, the restoration of low illumination regions, global and local measures of contrast.

##### 4.2.1. Entropy

Entropy is a statistical measure of the amount of information contained in an image. A high value, corresponding to the full use of permitted intensities, denotes a better image quality [7]. The entropy is given by Eq. (24).

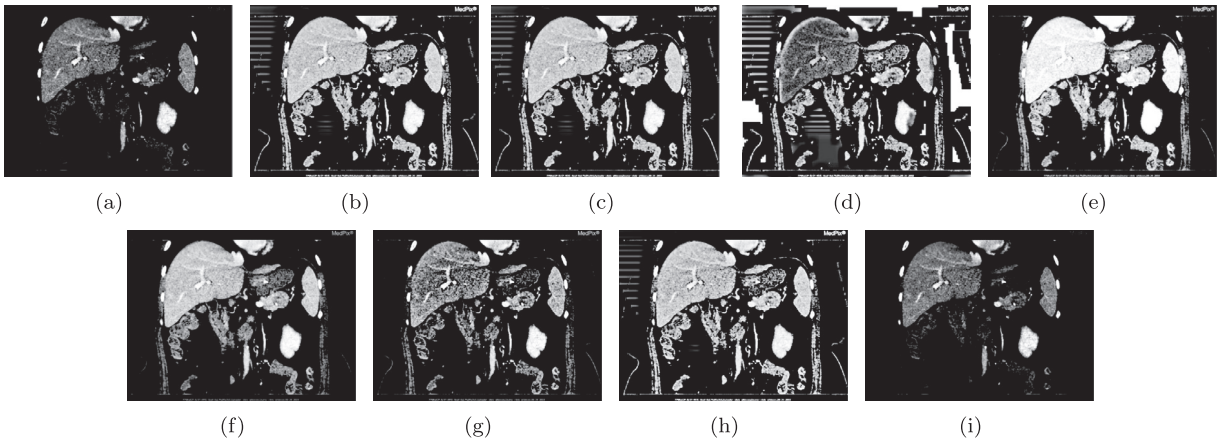


**Fig. 6.** Test image 5. (a) Input, (b) INDANE, (c) AINDANE, (d) NTFLA, (e) AGCCID, (f) AGCCPF, (g) SVLM, (h) LTISN, (i) ELIOHTP.

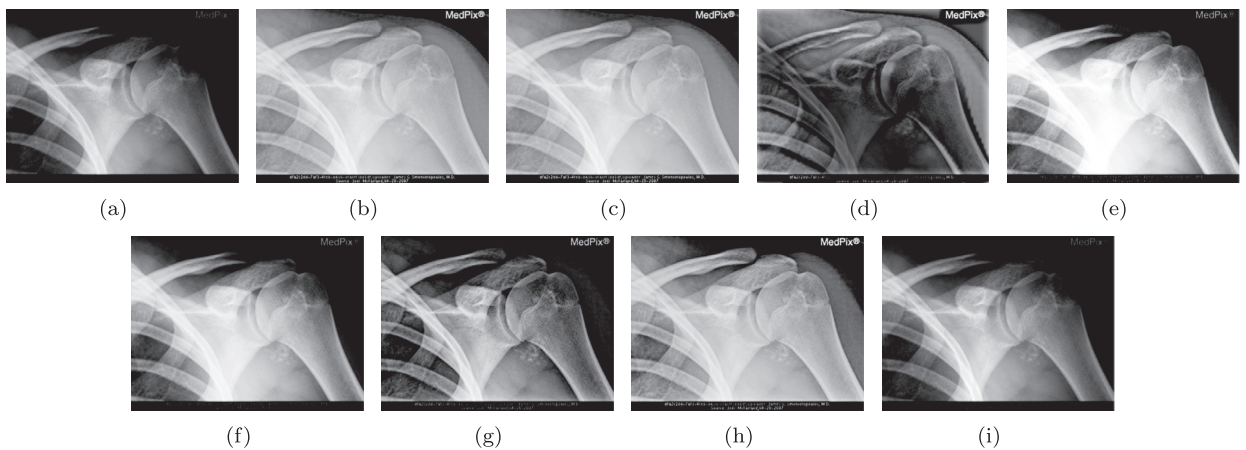


**Fig. 7.** Test image 6. (a) Input, (b) INDANE, (c) AINDANE, (d) NTFLA, (e) AGCCID, (f) AGCCPF, (g) SVLM, (h) LTISN, (i) ELIOHTP.

#### 4.2.2. Brightness

This performance index is the average brightness of an image [7]. Since the objective in this work is to restore images of low illuminations, a higher value signifies a better performance. Brightness is given by

$$\mathcal{B} = \frac{1}{XY} \sum_{\mathbf{x}} \overline{\text{RGB}}(\mathbf{x}), \quad \overline{\text{RGB}}(\mathbf{x}) = \frac{1}{3} \{R(\mathbf{x}) + G(\mathbf{x}) + B(\mathbf{x})\}. \quad (26)$$

#### 4.2.3. Contrast

This is a global measure of the average diversity of intensities. A large value means an image of better contrast [7]. It is determined from

$$\mathcal{C} = \frac{1}{XY} \sum_{\mathbf{x}} \overline{\text{RGB}}^2(\mathbf{x}) - \left( \frac{1}{XY} \sum_{\mathbf{x}} \overline{\text{RGB}}(\mathbf{x}) \right)^2. \quad (27)$$

#### 4.2.4. Gradient

The gradient is an average measure of the local difference between neighboring pixel intensities. A high gradient means the image is able to carry fine object details [7]. This performance measure is calculated from

$$\mathcal{G} = \frac{1}{XY} \sum_{\mathbf{x}} \sqrt{G_x^2(\mathbf{x}) + G_y^2(\mathbf{x})}, \quad (28)$$

where  $G_x(\mathbf{x}) = \overline{\text{RGB}}(x, y) - \overline{\text{RGB}}(x-1, y)$ , and  $G_y(\mathbf{x}) = \overline{\text{RGB}}(x, y) - \overline{\text{RGB}}(x, y-1)$ .

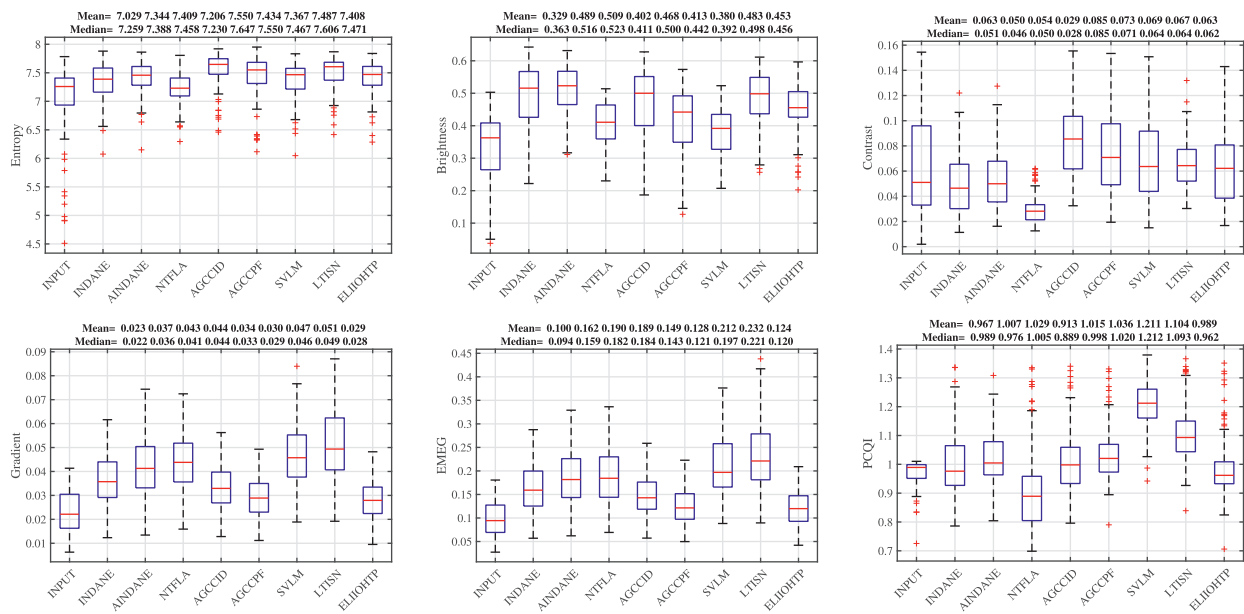


Fig. 8. Test result statistics.

#### 4.2.5. Expected measure of enhancement by gradient (EMEG)

This is a measure of the averaged ratio of block-based minimum absolute derivative to the maximum absolute derivative [25].

$$\text{EMEG} = \frac{1}{k_1 k_2} \sum_{i=1}^{k_1} \sum_{j=1}^{k_2} \frac{1}{255} \max \left( \frac{I_{en}(i, j)^{d_u^+}}{I_{en}(i, j)^{d_u^-} + \epsilon}, \frac{I_{en}(i, j)^{d_v^+}}{I_{en}(i, j)^{d_v^-} + \epsilon} \right), \quad (29)$$

where  $k_1, k_2$  are the number of blocks of size  $8 \times 8$ , superscripts  $d_u, d_v$  denote the derivative in horizontal and vertical directions, symbols '+' and '-' represent the maximum and minimum values of the derivatives in each block, and  $\text{EMEG} \in [0, 1]$ . This criterion measures the image sharpness; however, it is sensitive to speckle noises.

#### 4.2.6. Patch-based contrast quality index (PCQI)

This metric also divides the processed image into  $M$  blocks and uses the input image as a reference [26]. It measures the contrast stretch, structure change and brightness variation.

$$\text{PCQI}(I_{in}, I_{en}) = \frac{1}{M} \sum_{m=1}^M q_i(I_{in,m}, I_{en,m}) q_c(I_{in,m}, I_{en,m}) q_s(I_{in,m}, I_{en,m}), \quad (30)$$

where  $q_i(\cdot, \cdot) = \exp(-|c_1^x - c_2^y|/\sqrt{N})$ ,  $q_c(\cdot, \cdot) = 4/\pi \times \tan^{-1}(|c_2^y|/|c_2^x|)$ ,  $q_s(\cdot, \cdot) = (c_2^y + \mathbf{r}^\top \mathbf{v}_2)/||c_2^y \mathbf{v}_2 + \mathbf{r}||$ ,  $\mathbf{r}$  is the residual signal perpendicular to both  $\mathbf{v}_1$  and  $\mathbf{v}_2$ ;  $N$  is the number of pixels in a block,  $c_1^x = \sqrt{N}\mu_x$ ,  $c_2^x = ||\mathbf{x} - \mu_x||$ ,  $\mathbf{v}_1 = \mathbf{1}/\sqrt{N}$ ,  $\mathbf{v}_2 = (\mathbf{x} - \mu_x)/||\mathbf{x} - \mu_x||$ ,  $c_1^y = \sqrt{N}\mu_y$ ,  $c_2^y = \mathbf{y}^\top \mathbf{v}_2$ ,  $\mathbf{x}$  and  $\mathbf{y}$  are pixels from blocks in  $I_{in}$  and  $I_{en}$  respectively, and  $\text{PCQI} \in [1, 2]$  and a higher value indicates better image quality.

### 4.3. Analysis

Results of quantitative performance measures of the 100 test images are collected from the experiment. Statistics are illustrated as box plots shown in Fig. 8.

As the result statistics indicate, the entropy for ELIOOHTP has a mean of 7.408 and a median of 7.471 both better than the input at a mean of 7.029 and median of 7.259. The highest entropy is obtained from the AGCCID at a mean of 7.555 and a median of 7.627. However, as seen in the qualitative analysis, the AGCCID approach produces unwanted viewing artifacts. This is noticeable, e.g. the upper region in Fig. 2(e). The lowest entropy is from NTFLA with a mean of 7.026 and a median of 7.230 just marginally better than the input images.

The brightness obtained from ELIOOHTP has a mean of 0.453 and median of 0.456 against the input at a mean of 0.329 and a median of 0.363. It is evident that the ELIOOHTP method is able to restore low illumination images. The highest brightness comes from AINDANE at a mean of 0.509 and a median of 0.523. On the other hand, the AINDANE method tends to amplify noises in extremely low illumination images, see Fig. 3(c) upper-left region. The least brightness is obtained from SVLM with a mean of 0.380 and a median of 0.392.

The ELIOHTP method gives the contrast at a mean of 0.063 and a median of 0.062. This criterion is comparable to the input at a mean of 0.063 and a median at 0.051. A higher median value indicates that most results from the ELIOHTP are improvements on the input. The highest contrast measure is from the AGCCID with a mean at 0.085 and median also at 0.085, but the AGCCID method produces poor qualitative viewing results, see the lower-right region in Fig. 4(e). The lowest value is resulted from NTFLA with a mean of 0.029 and a median of 0.028.

The local gradient obtained from ELIOHTP has a mean of 0.029 and a median of 0.028, both are higher than the input at a mean of 0.023 and a median of 0.022. The highest gradient is obtained from LTISN at a mean of 0.051 and median of 0.049. Similar to other methods, LTISN produces artifacts and amplifies noises as found in Figs. 2(h) and 3(h). A low value gradient is obtained from AGCCPF with a mean of 0.030 and a median of 0.029.

The EMEG metric from ELIOHTP has a mean value of 0.124 and median of 0.120. The input image has a mean value of 0.100 and median of 0.094, both less than the result from ELIOHTP. Results from AGCCPF has a mean of 0.128 and median of 0.121, being comparable to ELIOHTP. It should be noted that, by referring to Figs. 2 and 3, AGCCPF results contain uneven and insufficient brightness amplifications respectively. Results from LTISN have the highest mean of 0.232 and median of 0.221. However, in Figs. 6 and 7, the medical images show un-necessary brightness amplification in unwanted regions.

With the assessment by PCQI, results from ELIOHTP have a mean of 0.989 and median of 0.962 comparable to the input image. It is also seen that ELIOHTP has an extended 3rd-quartile above that of the input images. The highest measure in PCQI is from SVLM with a mean of 1.104 and median of 1.093. However, SVLM results have the lowest brightness value and artifacts are generated in Figs. 6(g) and 7(g).

From the result statistics, it can be seen that there is not a single algorithm that has overall high quantitative measures. Furthermore, there is also not a common set of metrics that can indicate all aspects of image quality, such as the indication of artifacts. On the other hand, the proposed ELIOHTP method does not generate artifacts against a wide range of image contents. This fact indicates that ELIOHTP is applicable for a wide range of images of different illumination conditions and contents.

## 5. Conclusion

An automatic and optimal approach for restoring low illumination images has been presented. The implementation is straight forward, without un-necessary complicated procedures. It is automatic and does not require user interventions. The algorithm design is based on mapping the input intensity to output intensity using a scaled and weighted hyperbolic tangent function where the weight is proportional to the original intensity. The mapping is able to boost low intensities while leaving high intensities unchanged. The algorithm is also made adaptive to operate on diversified image contents by setting its parameter through the optimization perspective using the efficient golden section search. Experiment results, from images of natural indoor/outdoor scenes and medical contents, have shown that the proposed method is performing better than or comparable with several available methods with regard to qualitative and quantitative measures with respect to increased brightness and information content.

## References

- [1] Imtiaz MS, Wahid KA. Color enhancement in endoscopic images using adaptive sigmoid function and space variant color reproduction. *Comput Math Methods Med* 2015. Article ID 607407, 19 pages, doi: 10.1155/2015/607407.
- [2] Fu X, Wang J, Zeng D, Huang Y, Ding X. Remote sensing image enhancement using regularized-histogram equalization and DCT. *IEEE Geosci Remote Sens Lett* 2015;12(11):2301–5.
- [3] Kwak H-J, Park G-T. Image contrast enhancement for intelligent surveillance systems using multi-local histogram transformation. *J Intell Manuf* 2014;25(2):303–18.
- [4] Peng Y, Wu T, Wang S, Kwok N, Peng Z. Motion-blurred particle image restoration for on-line wear monitoring. *Sensors* 2015;15(4):8173–91.
- [5] Xu Y, Fang G, Lv N, Chen S, Zou JJ. Computer vision technology for seam tracking in robotic GTAW and GMAW. *Robot Comput Integr Manuf* 2015;32:25–36.
- [6] Kwok N, Shi H, Fang G, Ha Q, Yu Y-H, Wu T, et al. Color image enhancement using correlated intensity and saturation adjustments. *J Mod Opt* 2015;62(13):1037–47.
- [7] Lin S, Wong C, Rahman M, Jiang G, Liu S, Kwok N, et al. Image enhancement using the averaging histogram equalization (AVHEQ) approach for contrast improvement and brightness preservation. *Comput Electr Eng* 2015;46:356–70.
- [8] Jiang G, Lin S, Wong C, Rahman M, Ren T, Kwok N, et al. Color image enhancement with brightness preservation using a histogram specification approach. *Optik* 2015;126(24):5656–64.
- [9] Lin S, Wong C, Jiang G, Rahman M, Ren T, Kwok N, et al. Intensity and edge based adaptive unsharp masking filter for color image enhancement. *Optik* 2016;127(1):407–14.
- [10] Wong CY, Liu S, Liu SC, Rahman MA, Lin SC-F, Jiang G, et al. Image contrast enhancement using histogram equalization with maximum intensity coverage. *J Mod Opt* 2016;63(16):1618–29.
- [11] Tao L, Asari VK. An integrated neighborhood dependent approach for nonlinear enhancement of color images. In: International conference on information technology: coding and computing, 2004. Proceedings. ITCC 2004, 2. IEEE; 2004. p. 138–9.
- [12] Tao L, Asari VK. Adaptive and integrated neighborhood-dependent approach for nonlinear enhancement of color images. *J Electron Imaging* 2005;14(4):043006.
- [13] Chiu Y-S, Cheng F-C, Huang S-C. Efficient contrast enhancement using adaptive gamma correction and cumulative intensity distribution. In: IEEE international conference on systems, man, and cybernetics (SMC), 2011. IEEE; 2011. p. 2946–50.
- [14] Jiang G, Wong C, Liu S, Rahman M, Ren T, Kwok N, et al. Image contrast enhancement with brightness preservation using an optimal gamma correction and weighted sum approach. *J Mod Opt* 2015;62(7):536–47.
- [15] Gupta B, Tiwari M. Minimum mean brightness error contrast enhancement of color images using adaptive gamma correction with color preserving framework. *Optik* 2016;127(4):1671–6.
- [16] Ghimire D, Lee J. Nonlinear transfer function-based local approach for color image enhancement. *IEEE Trans Consum Electron* 2011;57(2):858–65.

- [17] Tsai C-Y. A fast dynamic range compression with local contrast preservation algorithm and its application to real-time video enhancement. *IEEE Trans Multimedia* 2012;14(4):1140–52.
- [18] Lee S, Kwon H, Han H, Lee G, Kang B. A space-variant luminance map based color image enhancement. *IEEE Trans Consum Electron* 2010;56(4):2636–43.
- [19] Arigela S, Asari VK. Self-tunable transformation function for enhancement of high contrast color images. *J Electron Imaging* 2013;22(2):023010.
- [20] Wong CY, Jiang G, Rahman MA, Liu S, Lin SC-F, Kwok N, et al. Histogram equalization and optimal profile compression based approach for colour image enhancement. *J Vis Commun Image Represent* 2016;38:802–13.
- [21] Yu C-Y, Ouyang Y-C, Yu T-W. Image contrast enhancement based on a three-level adaptive inverse hyperbolic tangent algorithm. *J Chin Inst Eng* 2013;36(1):103–13.
- [22] Geem ZW, Kim JH, Loganathan G. A new heuristic optimization algorithm: harmony search. *Simulation* 2001;76(2):60–8.
- [23] Yang X-S. A new metaheuristic bat-inspired algorithm. In: Nature inspired cooperative strategies for optimization (NISCO 2010); 2010. p. 65–74.
- [24] Karaboga D, Basturk B. A powerful and efficient algorithm for numerical function optimization: artificial bee colony (ABC) algorithm. *J Global Optim* 2007;39(3):459–71.
- [25] Celik T. Spatial entropy-based global and local image contrast enhancement. *IEEE Trans Image Process* 2014;23(12):5298–308.
- [26] Wang S, Ma K, Yeganeh H, Wang Z, Lin W. A patch-structure representation method for quality assessment of contrast changed images. *IEEE Signal Process Lett* 2015;22(12):2387–90.

**San Chi Liu** is a Ph.D. candidate and an Australian Postgraduate Awards scholar in the School of Mechanical and Manufacturing Engineering. He received his B.Eng. in mechatronic engineering from the University of New South Wales in 2012. His research interest includes machine learning and image process, with a focus on shadow removal in images.

**Shilong Liu** received his master degree in mechatronic engineering at Beijing Institute of Technology, China, in 2014. He is now a Ph.D. student in mechanical and manufacturing engineering at the University of New South Wales, Australia. His main research interests are image processing, computer vision and applied mathematics.

**Hongkun Wu** received his bachelor and master degree in mechanical engineering from Xi'an Jiaotong University, China, in 2012 and 2015. He is now a Ph.D. student in mechanical and manufacturing engineering at the University of New South Wales, Australia. His main research interests include image processing and machine condition monitoring.

**Md Arifur Rahman** received his B.Sc. degree in electrical and electronic engineering from Bangladesh University of Engineering and Technology, Bangladesh in 2007. He had worked as professional engineer in Ericsson before he completed his Ph.D. in the University of New South Wales, Sydney, Australia in 2017. His major research interests include machine vision, robotics and control system.

**Stephen Ching-Feng Lin** received his mechatronic engineering degree from the School of Mechanical and Manufacturing Engineering at the University of New South Wales, Australia, in 2010. Following his studies, he obtained the Ph.D. degree in Mechatronic Engineering from the same university in 2015. His major research interests include image processing, robotics and optimization algorithms.

**Chin Yeow Wong** acquired a Bachelor of Engineering (mechatronics) degree from the School of Mechanical and Manufacturing Engineering at the University of New South Wales, Australia, in 2010. He received a Doctor of Philosophy (mechatronics) degree at the same university in 2016. His major research interests are in image processing, human-computer interaction applications, and natural language processing.

**Ngaiming Kwok** received the M.Phil. degree from Hong Kong Polytechnic University, China, in 1997 and Ph.D. degree from University of Technology Sydney, Australia, in 2007. He is now with the University of New South Wales, Australia. His research interests include image processing, intelligent computation and automatic control.

**Haiyan Shi** obtained the M.Sc. degree and the Ph.D. degree in control theory and control engineering from Zhejiang University of Technology, Hangzhou, China in 2010 and 2013 respectively. She is with the School of Mechanical and Electrical Engineering, Shaoxing University, since 2000. Her research interests include wireless sensor networks, image processing and intelligent computation.